JTTEE5 8:133-145

Thermal Sprayed Titanium Anode for Cathodic Protection of Reinforced Concrete Bridges

S.D. Cramer, B.S. Covino, Jr., G.R. Holcomb, S.J. Bullard, W.K. Collins, R.D. Govier, R.D. Wilson, and H.M. Laylor

(Submitted 13 June 1998; in revised form 21 September 1998)

Stable operation of cobalt catalyzed thermal sprayed titanium anodes for cathodic protection (CP) of bridge reinforcing steel was maintained in accelerated tests for a period equivalent to 23 years service at Oregon Department of Transportation (Oregon DOT) bridge CP conditions with no evidence that operation would degrade with further aging. The cobalt catalyst dispersed into the concrete near the anode-concrete interface with electrochemical aging to produce a more diffuse anode reaction zone. The titanium anode had a porous heterogeneous structure composed of α-titanium containing interstitial oxygen and nitrogen, and a fcc phase thought to be Ti(O,N). Splat cooling rates were 10 to 150 K/s, and microstructures were produced by equilibrium processes at the splat solidification front. Nitrogen gas atomization during thermal spraying produced a coating with more uniform composition, less cracking, and lower resistivity than using air atomization.

Keywords anode properties, cathodic protection, infrastructure, reinforced concrete, thermal spray, titanium anode

1. Introduction

Reinforcing steel corrosion is the principal cause of concrete bridge structural deterioration in coastal marine environments and in areas where deicing salts are used for snow and ice removal. Steel corrosion products have molar volumes 1.5 to 3 times greater than the steel consumed by the corrosion reaction (Ref 1). These corrosion products produce tensile stresses within the concrete that cause it to crack (Ref 2), leading to concrete delamination and further steel corrosion. Cathodic protection (CP) is the most effective means for retarding, if not halting, these processes in steel-reinforced concrete structures in high chloride environments (Ref 3).

Thermal sprayed anodes for CP of reinforced concrete bridges are of recent origin, first developed in the United States by the California Department of Transportation (CALTRANS) (Ref 4), and increasingly being used by the Oregon Department of Transportation (Oregon DOT) (Ref 5, 6) and other state departments of transportation. Thermal sprayed anodes provide superior current distribution to reinforcing steel compared to other anode systems. They are applicable to complex shapes. Their installation has little impact on the aesthetic and structural integrity of bridges and is cost effective.

Consumable thermal sprayed zinc anode CP systems have been installed on three major Oregon bridges on coastal highway U.S. 101 (Ref 7). Accelerated laboratory electrochemical aging studies with periodic wetting of the anode (Ref 8, 9) indicated anode service lives of 25 to 27 years (Ref 10) based on anode-to-concrete bond strengths and anode consumption rates. The long term performance of the anode and the zinc-concrete interfacial reaction layer that forms with aging and affects the circuit resistance of the CP system are strongly dependent upon the presence of moisture at the anode-concrete interface (Ref 8, 9, 11).

A cobalt-catalyzed, nonconsumable, thermal sprayed titanium anode has recently been proposed as an alternative to thermal sprayed zinc anodes for impressed current cathodic protection (ICCP) systems (Ref 12, 13). Initial characterization of the structure of the anode (Ref 14, 15) and the results of accelerated laboratory electrochemical aging (Ref 16) have been reported. A field demonstration of the catalyzed thermal sprayed titanium anode was conducted at the Depoe Bay Bridge (OR) by the Oregon DOT and the Federal Highway Administration (Ref 14).

Thermal sprayed titanium coatings are typically applied in an inert atmosphere or vacuum using shrouds or chambers to prevent reactions with atmospheric gases (Ref 17). This is not practical with large outdoor structures. In this study, thermal sprayed titanium anodes were applied using either air or nitrogen (N_2) as the atomizing gas (Ref 14). An understanding of the mechanical, electrical, and electrochemical properties of the titanium anode requires an understanding of the significant titanium-atmospheric gas reactions and their effect on the chemistry, mineralogy, and structure of the anode. Furthermore, electrochemical aging may affect the anode properties or, as was found with the thermal sprayed zinc anodes, the chemistry of the anode-concrete interface (Ref 18). The aim of this paper is to present the chemistry, mineralogy, and structure of the titanium anode and the effects of electrochemical aging on anode operating properties and anode-concrete interfacial chemistry.

2. Experimental Procedure

2.1 Selected Properties of Ti-O-N Systems

Table 1 shows property data for compounds that could form during thermal spraying of titanium using air or N_2 as the atomizing gas (Ref 14). These data are useful for understanding the

S.D. Cramer, B.S. Covino, Jr., G.R. Holcomb, S.J. Bullard, W.K. Collins, R.D. Govier, and **R.D. Wilson,** Albany Research Center, U.S. Department of Energy, Albany, OR 97321; and **H.M. Laylor,** Research Unit, Oregon Department of Transportation, Salem, OR 97310.

chemistry, structure, and performance of the thermal sprayed titanium anode. The volume ratio in Table 1 is the ratio of the compound molecular volume to the atomic volume of the equivalent amount of metallic titanium in the compound.

Figure 1 shows the equilibrium phase diagram for the binary titanium-oxygen system (Ref 19) for illustrative purposes. The titanium-rich end of the phase diagram (0 to 13.5 wt% O) includes two metallic phases, a high-temperature β-titanium phase and an α-titanium phase stable at lower temperatures. Oxygen is soluble as an interstitial in the α-titanium and β-titanium structures throughout this region. The titanium-rich end of the titanium-nitrogen phase diagram is similar to the titanium-oxygen phase diagram, but freezing temperatures are substantially higher (Ref 20).

2.2 Unaged Anode Characterization

Anode characterization steps included (a) identification of phases present and their relative abundance, (b) quantification of interstitial oxygen and nitrogen in the metallic titanium phases, and (c) definition of the anode coating structure. It was also important to determine if there were benefits from using N_2 as the atomizing gas compared to air.

Anode Application. Thermal sprayed titanium anodes were applied using the twin-wire, arc-spray process (Thermion Bridgemaster 5100 series machine; Thermion Metallizing Systems, Silverdale, Washington). The feed wire was 3.2 mm (⅛ in.) diameter annealed grade 1 titanium wire. Spray parameters were electric arc, 36 to 40 V_{dc} and 300 A; atomizing gas, air or N_2 at 0.62 to 0.76 MPa (90 to 110 psi); spray orientation, normal to surface at a distance of 15 to 23 cm (6 to 9 in). The final titanium anode thickness was 50 to 150 μm (2-6 mils).

Field application to the bridge surface was performed with a hand-held spray gun. Laboratory application to concrete slabs (5 cm thick), concrete plates (1.5 cm thick), and borosilicate glass plates was performed with the same hand-held spray gun mounted to an Oregon DOT robotic XY traversing device to achieve a more uniform coating thickness than hand spraying.

Table 1 Selected properties of anode constituents

Property	Ti	TiO	TiO_2	TiN
Melting point, °C	1660	1750	1840	2930 (N liberated)
Theoretical density, g/cm^3	4.50	4.93	4.25	5.44
Volume ratio	1.00	1.20	1.73	1.09
Conduction type	Metallic	Metallic	N-type	N-type
Resistivity, μΩ · cm	50, 42(a)	350	$>3 \times 10^7$	15.5, 21.7(a)
Linear thermal expansion coefficient, μm/m · °C	8.5	…	9.4	8.0
Thermal conductivity, J/s · cm · °C	0.207	…	0.0653	0.242

(a) Values from two references. Source: Ref 14

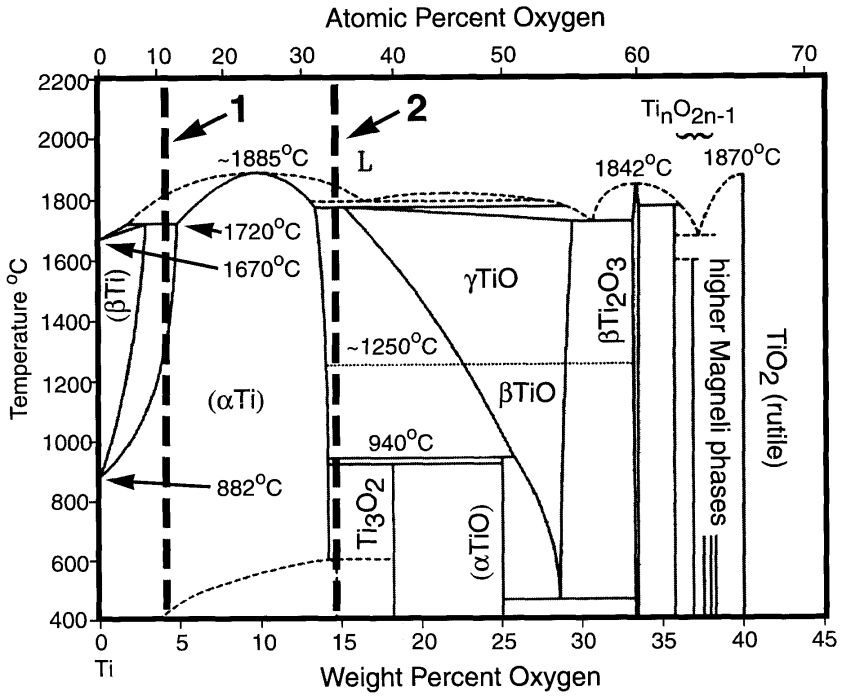

Fig. 1 Titanium-oxygen equilibrium phase diagram (Ref 14-19). Lines 1 and 2 were added, corresponding to cooling curves for alloy compositions with 88 and 66 at.%Ti, respectively.

Prior to spraying, concrete surfaces were lightly sandblasted to expose some aggregate and yield a medium sandpaper surface texture, and then blown free of dust. The borosilicate glass plates were degreased but not etched. Surfaces were not preheated prior to spraying.

Sample Preparation. Anode coatings used in the characterization studies were examined in situ by cutting a sample cross section with a diamond saw, which included the substrate and attached coating. Other samples were coating flakes chipped from the substrate surface. Cross-sectioned samples were mounted in epoxy to expose the cut anode edge and polished to a 1 μm diamond finish. Anodes prepared using N_2 atomization had good conductivity and did not require carbon coating prior to electron beam microanalysis; anodes prepared using air atomization were carbon coated.

Characterization Techniques. Scanning electron microscopy (SEM) images were obtained with secondary electrons (SE) and back-scattered electrons (BE). Elemental chemistry of the anode was determined using analytical scanning electron microscopy (ASEM) for selected spots on anode cross sections. X-ray fluorescence (XRF) microanalyses were performed using a wavelength dispersive spectrometer with four crystals and an energy dispersive spectrometer (EDS) with an atmospheric thin window for detection of low atomic number elements.

Crystallographic phases were determined by x-ray diffraction (XRD). The instrument was equipped with an automated goniometer, copper x-ray tube, variable divergence slit, focusing graphite monochromator, and a scintillation counter. X-ray diffraction analyses were performed on samples with the anode coating attached to the substrate (in situ) and on coating flakes stripped from the substrate and ground to a fine powder. Crystallographic structure was determined by precise measurements of anode lattice parameters using the National Institute of Standards Technology (NIST) 640 silicon powder "d" spacing standard. The measurement error for lattice parameters was ±0.001 Å for the powder samples and a factor of two to three times larger for the in situ samples.

The chemistry of the anode exterior surface was determined by a combination of x-ray photoelectron spectroscopy (XPS), using a 600 μm spot size, and argon ion sputter etching at a rate of 0.7 Å/s (based on SiO_2). This combination produced profiles of composition versus depth in the outer 0.2 μm of anode surface. Survey scans were performed to determine the elements present and their binding energies. Based on the adventitious carbon peak, there was no evidence of charging of the samples during XPS analysis.

The resistance of the anode during coating application and during electrochemical aging was measured with a spring-loaded, multipin probe (developed by Oregon DOT) and an alternating current-resistance meter (Ref 14). A four-point measurement technique was used to eliminate contact resistance. Anode thickness was measured using SEM photomicrographs of anode cross sections. Anode resistivity was computed from these measurements.

2.3 Anode Electrochemical Aging

Electrochemical aging was studied using catalyzed titanium anodes thermal sprayed on concrete slabs containing a steel mesh cathode. The experiments were conducted to determine changes occurring in anode bond strength, resistivity, and mechanical durability as a consequence of passing an electrical charge across the anode-concrete interface. In addition, measurements were made to determine the effect of aging on the chemistry of the anode-concrete interface and on anode operating performance and service life.

The catalyzed titanium anode serves solely as a current carrier to distribute charge to the reinforcing bar and as a support for the cobalt catalyst. In a basic environment, such as unaged concrete, the anode reaction is:

$$4OH^- \rightarrow 0_2 + 2H_20 + 4e^- \quad \text{(Eq 1)}$$

The consequence of this reaction is the loss of hydroxyl ions at the anode-concrete interface and a decrease in the interfacial pH. As this reaction progresses and the interface loses its basic character, the reaction becomes:

$$2H_2O \rightarrow O_2 + 4H^+ + 4e^- \quad \text{(Eq 2)}$$

Water is a key constituent in both of these reactions, in the first reaction as a source of replenishing hydroxyl ions produced by ionization of water and in the second reaction as the primary reactant. Consequently, delivery of moisture to the anode by humid air, dew, fog, and precipitation is crucial to successful operation of the anode.

Laboratory Aging Experiment. Laboratory concrete slabs were prepared to physically and mechanically approximate a section of a reinforced concrete structure in a thermal sprayed titanium anode cathodic protection system (Fig. 2). The concrete slabs measured 23 by 33 by 5 cm (9 by 13 by 2 in.) and were cast with 3.2 cm (1.25 in.) concrete cover over No. 16 expanded steel mesh simulating the rebar. The concrete mix design approximated that used in Oregon's coastal bridges in the 1930s and had a water-cement ratio of 0.48. Sodium chloride was added to the concrete mix at 3 kg NaCl/m^3 (5 lb NaCl/yd^3) of concrete to approximate the present salt content of older coastal bridges in Oregon. Slabs were cured for four weeks in a moist room, then air dried for one week. The top surface of each slab was prepared in the same way as concrete surfaces in the anode characterization part of the study, by sandblasting and then blowing free of dust. Prior to thermal spraying, the area around the wire that leads to the steel mesh was masked off to a distance of 2.5 cm to prevent electrical contact between the lead wires and the titanium anode to be applied. The slab surface was then thermal sprayed with titanium using robotic control and the same application conditions used in the anode characterization part of the study.

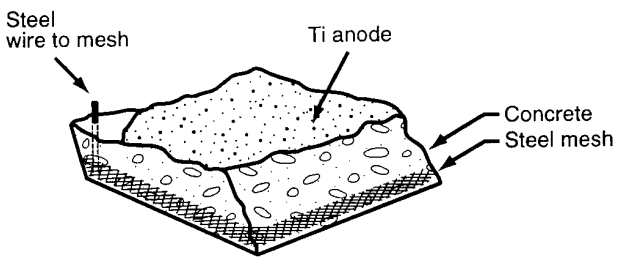

Fig. 2 Construction of laboratory concrete slabs

The titanium anode was catalyzed using a cobalt-nitrate-amine complex, which was converted to cobalt oxide, Co_3O_4, during its application as an aqueous acidic solution (pH 3.47). The solution consisted of divalent and trivalent cobalt, contained a total of 60 g Co/L, with the divalent cobalt present as cobalt nitrate, the trivalent cobalt present as an amine complex, and a Co(III)/Co(II) ratio of 0.25. It was applied to the anode with the ICCP system operating, that is, with the titanium anode polarized anodically to the rebar. Impressed current cathodic protection operation was continued for a minimum of 72 h after catalyst application (Ref 14). In this way, the cobalt absorbed into pores of the anode and cement paste was converted to the active catalyst, Co_3O_4. The Co_3O_4 had a spinel structure with the divalent ion in the tetrahedral interstices, and the trivalent ion in the octahedral interstices (Ref 1, 21), was a p-type semiconductor (Ref 1, 22), and was a highly active catalyst for surface reactions involving oxygen (Ref 22, 23).

The cobalt catalyst was brush applied to the titanium anode at full strength and at an application rate of 0.344 L/m^2 (0.0087 gal/ft^2) approximately two months after the slabs were thermal sprayed. Catalyst application was done with the titanium anode polarized anodically to the steel mesh at a current density of 29 mA/m^2 (2.7 mA/ft^2). Anodic polarization of the titanium anode was continued for a period of one month. Anodes on four concrete slabs were catalyzed in this way. A fifth slab was used as a control and had no catalyst applied to the anode.

Electrochemical aging (Ref 5-11, 18) of the laboratory anodes was conducted at a current density of 21 mA/m^2 (2 mA/ft^2), and the anodes were aged to a total charge of 1520 kC/m^2 (39.2 A · h/ft^2). (A multiplying factor of 0.0258 converts kC/m^2 to A · h/ft^2.) This was an accelerated rate compared to current densities typically used by the Oregon DOT for coastal ICCP systems (2.1 mA/m^2, or 0.2 mA/ft^2), and the total charge was equivalent to approximately 23 years anode service on a coastal bridge. Aging was conducted in a controlled environment room at approximately 24 °C and 75 to 90% relative humidity (RH), except during one period when the room RH was varied several times from 30 to 100%. The slabs were periodically wetted with deionized water to simulate the wet-dry cycles experienced by coastal bridges exposed to rain, fog, and dew.

Field Aging Experiment. The Depoe Bay Bridge (OR) on U.S. Highway101 consists of the original 1926 reinforced concrete structure and a reinforced concrete widening bridge built in 1939. Installation of a consumable zinc anode CP system was completed in early 1996. However, in this project, a 280 m^2 (3015 ft^2) cobalt-catalyzed, thermal sprayed titanium anode was installed in CP zone 14 on the bridge (Ref 14). Anode application parameters were the same as for the laboratory slabs with the following exceptions: the atomizing gas was air, and application was by means of a hand-held spray gun.

The field titanium anode was catalyzed with the same cobalt catalyst used in the laboratory aging experiments. The catalyst was pressure sprayed as an aqueous acidic solution onto the titanium anode in three coats, the first two coats at full strength and the final coat as a 1 to 1 dilution. The total application was 0.344 L/m^2 (0.0087 gal/ft^2) of full strength catalyst. A minimum of 30 min drying time was allowed between each coat. During application, the anode was polarized at a current density of 10.8 mA/m^2 (1.0 mA/ft^2) with the titanium anodic to the rebar. As an ICCP system, zone 14 was operated at a current density of 2.8 to 3.8 mA/m^2 (0.26 to 0.35 mA/ft^2) with a voltage of between 1.4 and 1.7 V. Two 5.1 cm (2 in.) diameter core samples were taken from the southwest corner of zone 14 after approximately 1.4 years of operation for purposes of characterizing the anode-concrete interface of the aged bridge anode. At the time of coring, the titanium anode electrochemical age was 146 kC/m^2 (3.8 A · h/ft^2).

Characterization Techniques. The electrochemically aged anode was characterized by the same techniques used to characterize the unaged anode. In addition, the strength of the anode bond to the concrete and the chemistry of the anode-concrete interface were determined. Bond strength was measured with a universal tensile testing machine and 5 cm diameter aluminum dollies (Ref 5-11, 18) epoxied to the anode surface.

The pH of the anode-concrete interface was measured using a temperature-compensated micro-combination pH electrode requiring as little as 0.1 mL of solution (Ref 18, 24). Standard soil pH methodology (Ref 25) was modified for the small size of the samples available from the anode-concrete interface. Pieces of the titanium anode were manually parted from the concrete using a thin blade. A drop of deionized water was applied to the side of the anode adjacent to the concrete and allowed to equilibrate 5 min with adhering concrete residues. The pH of the water drop was then measured. The same procedure was used on scrapings removed from the concrete surface exposed during removal of the anode. These scrapings were formed into a slurry with a drop of deionized water. They represent a volume of interface immediately adjacent to the residues adhering to the anode and displaced from them by roughly 0.1 mm. The pH measured on the concrete side of the interface (scrapings) was typically higher by ½ to 1 full pH unit from that measured on the anode surface due to the buffering action of the increased amount of unaltered cement paste in the slurry sample.

3. Results and Discussion

3.1 Unaged Anode Characterization

Titanium anodes, formed using either N_2 or air atomization, are built up of individual molten droplets that impact the surface being coated, spread over it to form "splats" as freezing structures develop, and weld to adjacent splats. Rough measurements of splat sizes in BE SEM images showed them to be 100 to 200 μm in width and 10 to 25 μm thick, with some larger and smaller than these sizes. These dimensions were typical of those for thermal sprayed coatings of many other materials (Ref 17).

X-Ray Diffraction. The primary crystalline phases present in the anode were the hexagonal close-packed (hcp) α-titanium and a face-centered cubic (fcc) structure similar to TiN and γ-TiO. The TiO_2 and the body-centered cubic (bcc) β-titanium were not detected.

X-ray diffraction measurements showed that the α-titanium lattice expanded. The lattice parameters of pure α-titanium, free of interstitial elements, were *a*-axis 2.950 Å and *c*-axis 4.682 Å, with a *c*/*a* ratio of 1.587 (Ref 24). Measured values for the thermal sprayed anodes were 2.973, 4.788, and 1.610 Å, respectively. They show the lattice was greatly expanded along the *c*-axis and indicate the α-titanium lattice contained substantial

oxygen and/or nitrogen dissolved in the hcp phase. The α-titanium saturation values were 22 at.% for nitrogen (Ref 26, 27) and 34 at.% for oxygen (Ref 28).

The measured *a*-axis for the fcc phase was 4.215 Å. The γ-TiO was the only titanium oxide that had a fcc structure. The *a*-axis for γ-TiO was 4.180 Å at 46 at.% oxygen and decreased with increasing oxygen content (Ref 28). The *a*-axis for the fcc TiN was 4.207 Å at 28.5 at.% nitrogen and increased with increasing nitrogen content (Ref 27). The likely structure for the fcc phase includes both oxygen and nitrogen, for example, Ti(O,N), and would represent a minimum in lattice energy generated by the inclusion of the larger nitrogen ion (1.71 Å radius) in the same structure as the smaller oxygen ion (1.32 Å radius) (Ref 29). A minimum lattice energy would correspond to a measured *a*-axis value intermediate between the values for the TiN and γ-TiO structures.

X-Ray Photoelectron Spectroscopy. Only titanium, oxygen, nitrogen, and carbon were detected on the anode surface in XPS survey scans. Carbon disappeared within the first 120 s of sputter etching, indicating it was adventitious carbon and not part of the anode chemistry. Figure 3 shows titanium XPS peaks as a function of sputter etching for the anode formed using N_2 atomization. The lowest curve in the figure corresponds to that produced by the unetched surface. Each succeeding curve was produced after sputter etching for 120 s. Twenty cycles of sputter etching are represented in Fig. 3, for a total analysis depth of 0.15 μm. At the very surface of the anode, the $Ti2p_{3/2}$ binding energy peak was at 459.3 eV, close to the value 458.8 eV characteristic of titanium in TiO_2 (Ref 30). After two or three sputtering cycles, this peak disappeared and a new $Ti2p_{3/2}$ peak emerged at 455.3 eV, which increased in height with each sputtering cycle. This peak is close to that for titanium in metallic titanium (454.2 eV), TiO (455.1 eV), and TiN (455.8 eV) (Ref 30), and the $Ti2p_{3/2}$ peak at 455.3 eV is the sum of contributions from TiO, TiN, and metallic titanium bonds. This would indicate titanium is present in the anode largely as metallic titanium and as Ti(II) with bonds to oxygen and nitrogen.

With sputtering, binding energy spectra for oxygen quickly transitioned from energies characteristic of TiO_2 to those of TiO. Spectra at binding energies characteristic of TiN (Ref 14) showed little nitrogen present at the anode surface, but nitrogen concentrations increased rapidly with sputter etching.

Figure 4 plots XPS spectral data for titanium anodes formed using N_2 atomization as a function of sputter etching to give the composition depth profile for the anode near-surface region. After several sputter cycles, oxygen decreased with increasing depth in the coating, while both nickel and titanium concentrations increased with depth. The anion-to-cation ratio, (O + N)/Ti, decreased from 2 at the surface (discounting contributions from carbon) to 1 at a depth of 0.1μm. This indicates a very thin outer region of TiO_2 that transitions quickly to a region composed of metallic titanium and Ti(O,N). This TiO_2 is present in such a small amount that it would be undetectable by XRD. The composition depth profile for anodes formed using air atomization had the same general features as Fig. 4. However, while the nitrogen curve was almost identical, the titanium curve was somewhat lower, and the oxygen curve was higher. As a consequence, the anion-to-cation ratio declined more slowly with depth, and the anode surface appeared more oxidized for anodes formed using air atomization.

Analytical SEM. Figure 5 shows typical views of thermal sprayed titanium anode cross sections on concrete for an anode formed using air atomization. Figures 5(a) and (b) are images of the same area viewed by SE and BE, respectively. The BE images clearly show the composition gradients (bright areas are regions with high average atomic number; dark regions are low atomic number) that define reaction zones developed between the initially molten or hot titanium and oxygen and nitrogen in air. The boundaries of individual splats are lined by these reaction zones and give the image a banded appearance. The dark regions are richer in oxidized titanium, that is, TiN, TiO, and/or Ti(O,N). The light regions are richer in α-titanium containing interstitial nitrogen and oxygen.

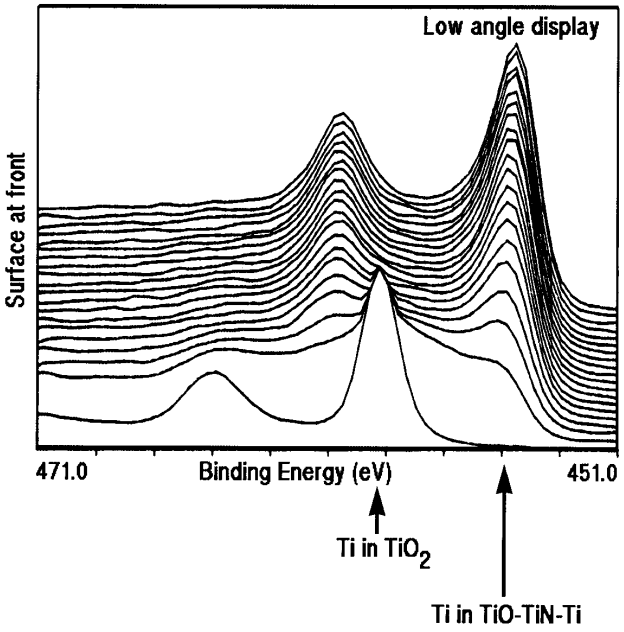

Fig. 3 $Ti2p_{3/2}$ and $Ti2p_{1/2}$ peaks as a function of sputter etching; anode formed using N_2 atomization

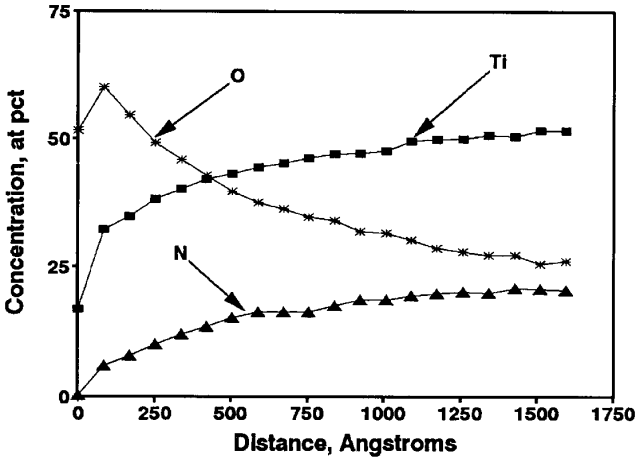

Fig. 4 X-ray photoelectron spectroscopy composition depth profile for anode formed using N_2 atomization

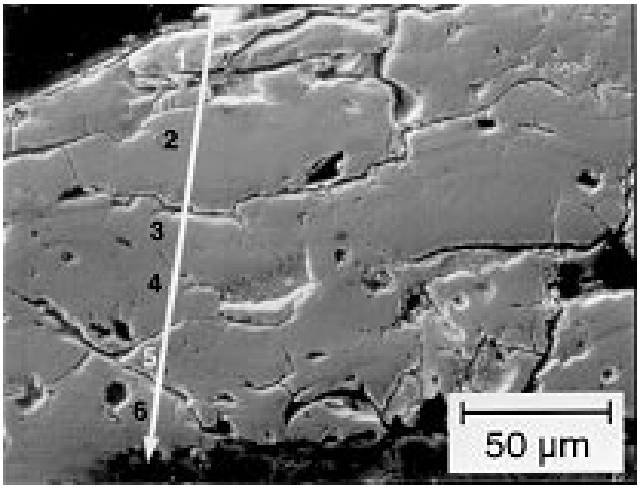

(a)

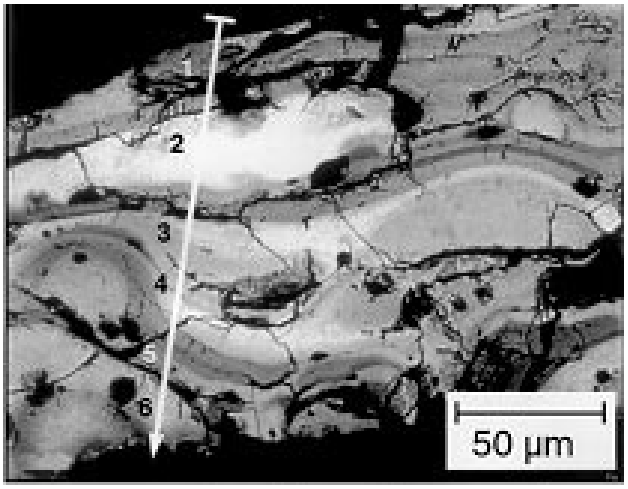

(b)

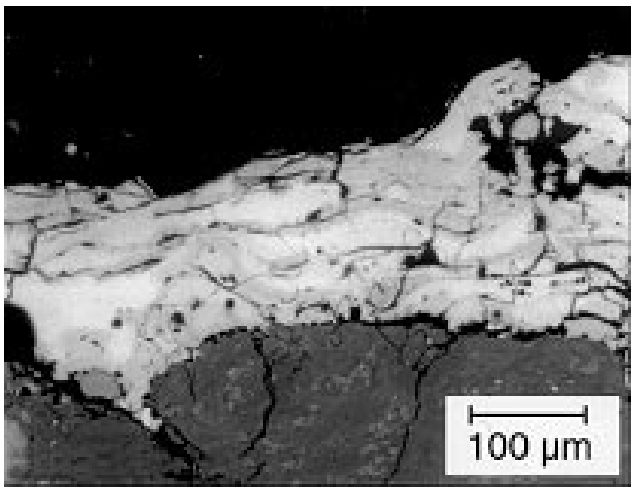

(c)

Fig. 5 Photomicrographs of polished cross section of anode thermal sprayed on concrete using air atomization. (a) Secondary electron image. (b) Back-scattered electron image of area in (a). (c) Back-scattered electron image

Primary cracks in the anode occurred in the heavily oxidized reaction zones at the interface between adjacent splats. These cracks were the source of secondary cracks that radiated from the interfacial cracks into and across splats to other reaction zones. Comparison with anodes formed using N_2 atomization showed the latter had a more uniform coating chemistry, and there was less primary and secondary cracking.

Figure 5(c) is a lower magnification view of the BE image in Fig. 5(b). It shows good conformation between the anode and the rough concrete surface. Penetration of the splats at the interface into surface roughness of the concrete in this way ensures a good initial mechanical bond for the anode.

The arrows in Fig. 5 define the path of a line scan to determine local composition of the anode. The numbers refer to individual splats distinguished in Fig. 5(b). Figure 6 shows the results of the line scan. Six splats are clearly defined by these results. The boundaries of the splats are characterized by a sharp rise in oxygen concentration and substantially reduced titanium and nitrogen concentrations. These results are qualitatively similar to those obtained by XPS for the anode surface (Fig. 4), that is, high oxygen and depressed titanium and nitrogen concentrations at the splat outer surface. The line scan results show that the splat chemistry between the boundaries, that is, the splat internal chemistry, is fairly uniform with measured oxygen and nitrogen levels of 10 to 20 at.% each and titanium levels of approximately 70 at.%.

Line scans were performed on a series of cross sections from anodes on concrete formed using air and N_2 atomization. The average anode composition was calculated as the mean of the values along these multiple scans (Table 2). Anodes formed using air contained more oxygen and less nitrogen and titanium than for those formed using N_2. The anion-to-cation ratio, (O + N)/Ti, was higher for air, 0.48, compared to N_2 atomization, 0.43. Based on a mass balance and the principle anode constituents, α-titanium and Ti(O,N), this suggests there is less metallic titanium in anodes formed using air rather than N_2 atomization. If much of the oxygen and nitrogen in the anode is present as interstitials in α-titanium (and the XRD results show this to be the case), it follows that more than 50 at.% of the titanium in the anode is present as metallic titanium, regardless of whether the anode was formed using N_2 or air atomization.

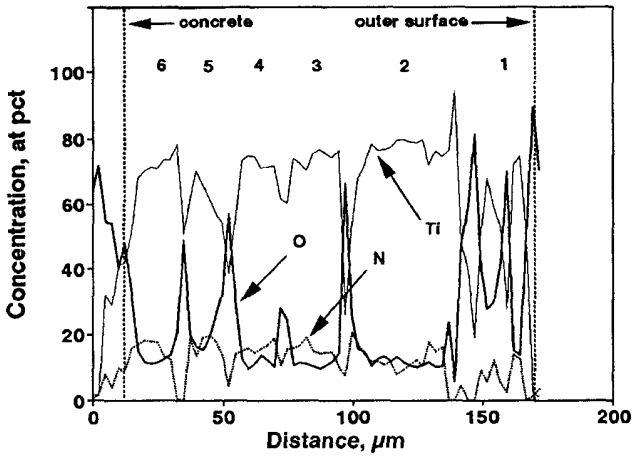

Fig. 6 Composition-depth profile along traverse indicated by arrow in Fig. 5(a) and (b). Anode formed using air atomization

Table 2 Average composition of anodes formed on concrete

Substrate and atomizing gas	Anode composition, at.%			Anion/cation ratio, (O + N)/Ti
	0	N	Ti	
Borosilicate glass, air	17.7	14.6	67.5	0.48
Concrete, air	19.3	13.0	67.5	0.48
Average	**18.5**	**13.8**	**67.5**	**0.48**
Borosilicate glass, nitrogen	13.2	17.1	69.6	0.43
Concrete, nitrogen	13.9	16.5	69.5	0.43
Average	**13.5**	**16.8**	**69.6**	**0.43**

Table 3 Composition of phases in anode freezing structures

Image Area	Area description	Composition, at.%			Anion/cation ratio, (O + N)/Ti
		O	N	Ti	
Fig. 7(b)—1	White	9.0	1.5	89.4	0.12
Fig. 7(a)—2	Light gray	12.4	18.0	69.5	0.43
Fig. 7(c)—3a	Light phase	28.4	15.7	55.9	0.79
Fig. 7(c)—3b	Dark phase	42.1	17.3	40.5	1.47
Fig. 7(d)—4a	Light phase	10.9	0	89.1	0.12
Fig. 7(d)—4b	Dark phase	8.7	9.0	82.3	0.22

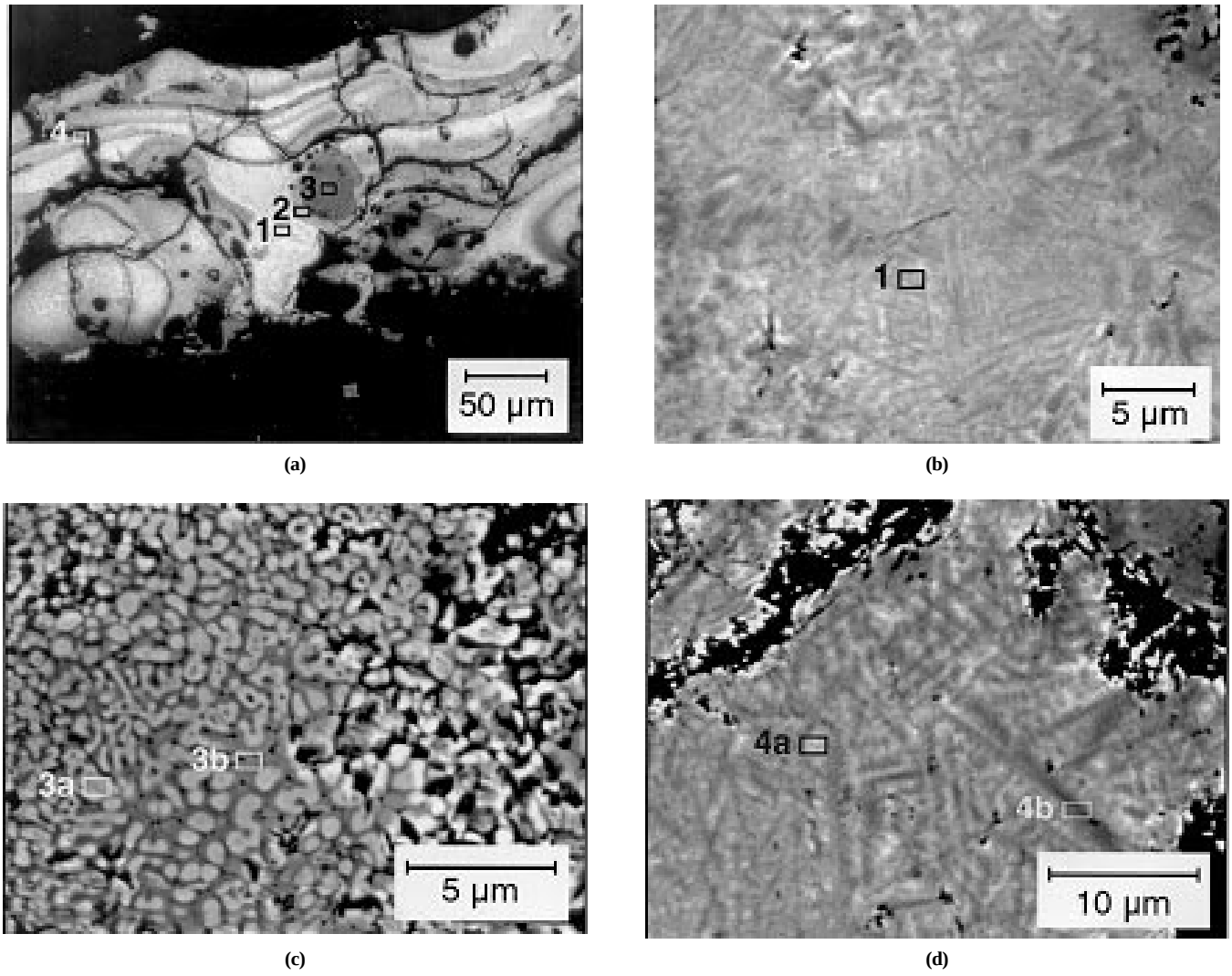

Fig. 7 Freezing structures in anode formed using air atomization. (a) Back-scattered electron image of anode cross section showing location of analysis areas 1 through 4. (b) Analysis area 1. (c) Analysis areas 3a and b. (d) Analysis areas 4a and b.

Solidification Processes. The microstructure of thermal sprayed anodes depends upon cooling rate and chemical composition. Equilibrium solidification typically occurs at cooling rates below 10^4 K/s for hcp materials such as titanium because of the low thermal conductivity associated with this crystal structure (Ref 31, 32). Above 10^4 K/s, rapid solidification processes can occur, and nonequilibrium metastable microstructures form, with the result being increased solute solubility and decreased grain size (Ref 33). Cooling rates were computed for molten titanium splats on titanium and concrete substrates, using both the thick and thin weld cooling rate equations (Ref 34). Computed cooling rates were low due to the fact that concrete is a poor heat sink and ranged from 10 to 150 K/s. These values were well below those leading to rapid solidification. Thus, local equilibrium was maintained at the melt/solid interface, and splat freezing structures are defined by the equilibrium phase diagram, for example, Fig. 1, and characterized by the composition and temperature at the solidification front (Ref 35).

Figure 7 shows typical anode freezing structures on concrete slabs. These correspond to compositions given in Table 3. Figure 7(a) shows the location of the areas imaged and analyzed. Figures 7(b) and (d) show structures formed following cooling curves similar to line 1 in Fig. 1 for the alloy with 88 at.% Ti. (Analogous structures formed, following a similar line in the binary titanium-nitrogen system.) The α-titanium dendrites were the first phase to freeze from the molten splats. With further cooling a peritectic reaction involving molten titanium and the α-titanium formed a second phase, β-titanium. Because diffusion in the solid phase was slow compared to diffusion in the molten titanium, the peritectic reaction did not proceed to completion, consuming only a fraction of the α-titanium, and segregation occurred with β-titanium coating the α-titanium dendrites. The β-titanium formed by the peritectic reaction contained lower concentrations of interstitial oxygen (and nitrogen) than the α-titanium initially formed (Table 3). As the solid structure cooled further, the β-titanium transformed to α-titanium because oxygen (and nitrogen) are α-titanium stabilizers. The XRD data showed this transformation was complete. Hence, in BE images 7(b) and (d), the dark dendrites are the initial α-titanium. The lighter interdendritic material is also α-titanium, which transformed from β-titanium and contains lower concentrations of interstitial oxygen (and nitrogen) than the dendrites.

The freezing process is substantially different when the melt contains much lower levels of titanium (<75 at.% Ti) and higher levels of oxygen. Figure 7(c) shows the structure formed following cooling curves similar to line 2 in Fig. 1 for the alloy with 66 at.% Ti. The α-titanium dendrites again were the first solid phase to freeze from the molten splats. With further cooling, fcc γ-TiO (or Ti(O,N)) freezes from the melt and coats the α-titanium dendrites. The α-titanium dendrites contain substantially less oxygen (and nitrogen) than the γ-TiO (Table 3). Thus, in BE image 7(c), α-titanium dendrites are the light phase, and the dark phase is interdendritic γ-TiO (or Ti(O,N)). The XRD data showed lower temperature titanium oxides, such as Ti_3O_2 or α-TiO, were absent from the freezing structures.

Table 4 Resistivity of titanium thermal sprayed on borosilicate glass plates

Atomizing gas	Resistivity, μΩ · cm	Ratio to air resistivity
Air	3562	1.00
Nitrogen	2160	0.61

Resistivity. Applicators of thermal sprayed titanium anodes commonly use anode resistance to determine when the coating is sufficiently conductive to meet design specifications (Ref 14). For service as an electrical conductor, designers of CP systems need an anode with low, uniform initial resistance and with a resistance that does not change significantly with electrochemical age.

Table 4 shows the resistivity of uncatalyzed, unaged coatings formed on borolsilicate glass plates and determined by measurement of coating resistance, area, and thickness. These values are significantly higher than those for constituents of the anodes, that is, α-titanium, γ-TiO, and TiN (see Table 1). They suggest that cracking within the anode, the heterogeneous anode composition, and the presence of Ti(O,N) have substantially degraded electron conduction paths within the anode.

The resistivity of anodes formed using N_2 atomization was 40% lower than that for anodes formed using air atomization. This lower resistivity agrees with the observation of less cracking, more uniform composition, and lower oxide (or Ti(O,N)) content for anodes formed using N_2 atomization. It suggests that N_2 atomization has benefits that directly affect anode application specifications and anode service as a current carrier. By extension, more uniform anode composition and structure, with less cracking and lower apparent resistivity, could also result by using a shroud to reduce air entrained in the N_2 used to atomize the molten titanium. Reduced levels of Ti(O,N) might also be achieved by doping the titanium with tungsten, tantalum, or niobium to change the semiconducting properties of the splat oxide skin. Such dopants increase the conductivity of the oxide, thereby reducing the oxidation rate of the titanium (Ref 36, 37).

3.2 Anode Electrochemical Aging

With the exception of the uncatalyzed anode, titanium anode performance in the laboratory was stable over the entire period the anodes were electrochemically aged, equivalent to 23 years service at Oregon DOT coastal ICCP conditions. The electrochemical performance continued relatively unchanged with aging for this period, while the mechanical durability of the anode surface deteriorated.

Electrochemical Performance. Figure 8 shows the voltage of catalyzed and uncatalyzed anodes on concrete slabs from the laboratory study as a function of electrochemical aging. For an age of 700 kC/m^2 (18.1 A · h/ft^2), equivalent to ten years service, the catalyzed and the uncatalyzed anodes performed essentially the same. For the uncatalyzed anode, this appeared to represent an induction period, and the slab voltage increased markedly thereafter with aging, depending upon the humidity and wetting of the anode. The first two peaks in the uncatalyzed anode curve (beginning at 700 kC/m^2) correspond to periods when the RH was decreased to 30% and then raised to 100%. The voltage of the uncatalyzed anode rose steadily beyond 1200 kC/m^2 (at a RH of 70 to 80%) and decreased only when the anode was periodically wetted with deionized water. In contrast, the voltage of the catalyzed anode varied little with longer aging or with wetting.

Slab voltage, V, is shown as a function of relative humidity (RH) in Fig. 9 for catalyzed and uncatalyzed anodes during the period when the laboratory humidity was varied. The voltage for the catalyzed anode increased fom 2.5 to 7.0 volts when the humidity decreased from 100 to 30 pct RH. The increase in voltage with decreasing RH was linear and very slight, indicating the catalyzed anode performance was not strongly dependent upon RH. Furthermore, it indicates sufficient water was delivered to the catalyzed anode from the environment to maintain the anode reaction without undue polarization of the anode. A least squares fit of the catalyzed anode data shows the humidity dependence of the slab voltage to be:

$$V = 6.98 - 0.0314\ RH \quad \text{(Eq 3)}$$

In contast, the voltage for the uncatalyzed anode rose sharply and to unacceptably high levels with decreasing RH. A least squares fit of the uncatalyzed anode data shows the humidity dependence to be:

$$V = 92.04 - 0.8172\ RH \quad \text{(Eq 4)}$$

This suggests the uncatalyzed anode has become passive and is exhibiting limited valve metal characteristics. It agrees with the work of others (Ref 38), where uncatalyzed titanium oxide films were considered for use as humidity sensors because they showed increased levels of ionic conduction when water absorbed on their surface.

Anode Properties. Table 5 shows the properties of unaged and aged anodes on concrete slabs. The resistivity of the unaged anode produced by air atomization was 10% lower after it was catalyzed. With aging, the resistivity of the uncatalyzed anode increased to almost three times that of the unaged anode. The resistivity of the catalyzed anode also increased with aging, but the increase was less than that of the uncatalyzed anode, that is, 7200 $\mu\Omega \cdot$ cm vs. 8280 $\mu\Omega \cdot$ cm. These changes may be due to microcracking within the anode as a result of the brittle nature of the coating and chemical and structural changes within the cement paste at the anode/concrete interface.

The resistivity of the unaged, catalyzed anode formed by N_2 atomization was 40% less than that of the same anode formed by air atomization, in agreement with the results for coatings formed on glass plates (Table 4). The resistivity of the catalyzed anode formed by N_2 atomization increased with aging, but again was 40% lower than that of the same anode formed by air atomization. Thus, aging results in an increase in anode resistivity, regardless of how the anode was formed or the prior treatment of the anode. The use of N_2 atomization (compared to air atomization) reduces resistivity substantially for both the unaged and aged anode.

The resistivity of the unaged, catalyzed Depoe Bay Bridge anode was similar to that measured for the unaged anode on concrete slabs. Like the anodes on concrete slabs, anode resistivity on the Depoe Bay Bridge increased with electrochemical age. After 2½ years of anode operation, equivalent to the passage of 215 kC/m^2 (5.6 A $\cdot$ h/ft^2) charge, the anode resistivity had increased by 15%.

The bond strength of unaged, uncatalyzed titanium anodes on concrete, sprayed using both air and N_2 atomization, averaged 1.18 ± 0.18 MPa (Ref 14). Bond strengths decreased substantially with aging. For example, the bond strength of the aged, uncatalyzed anode was negligible, and the anode was friable and easily damaged by abrasion. The bond strength of the aged, catalyzed anode was approximately 25% that of the

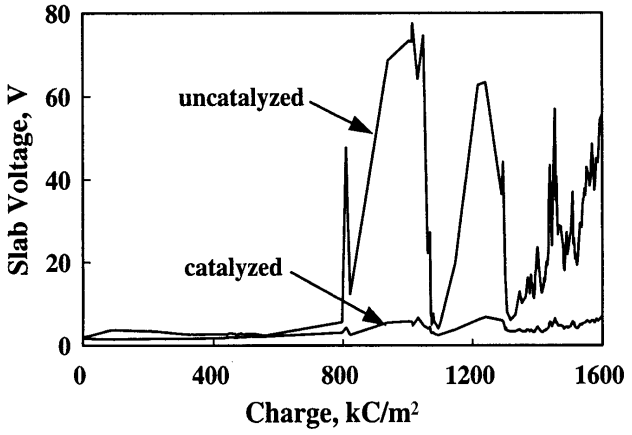

Fig. 8 Slab voltage as a function of electrochemical age (in kC/m^2)

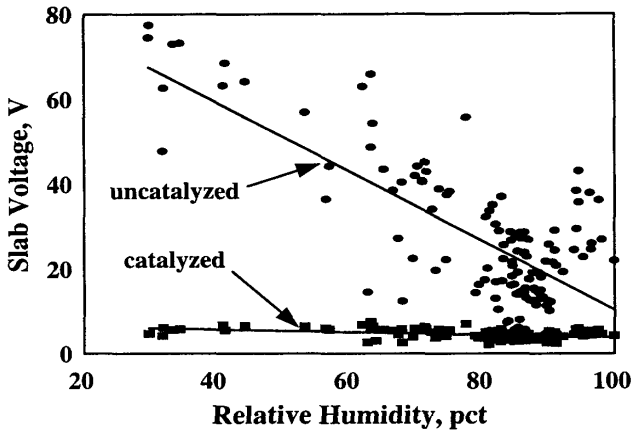

Fig. 9 Voltage requirements of thermal sprayed titanium anode as a function of relative humidity. Anode current density 21.5 mA/m^2

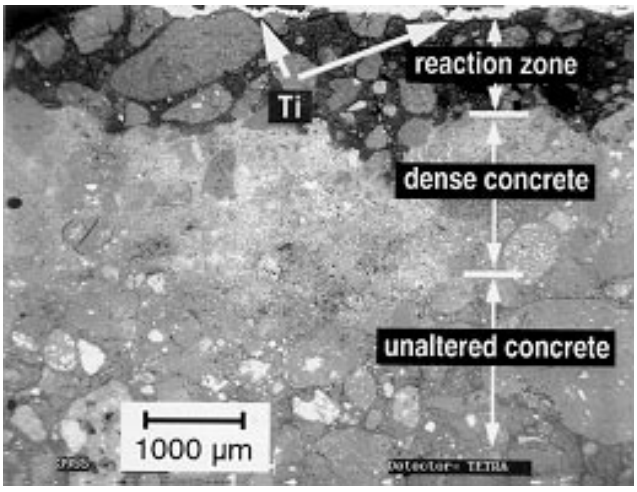

Fig. 10 Back-scattered electron scanning electron micrograph of cross section of aged, catalyzed anode formed using air atomization

unaged anode, but superior to that of the aged, uncatalyzed anode. While the aged, catalyzed anode was also friable, it was more durable and less easily damaged by abrasion than the aged, uncatalyzed anode. The bond strength of aged anodes formed using N_2 atomization was marginally higher than that of aged anodes formed using air atomization. However, loss of bond strength on aging did not result in loss of coating from the concrete surface except when the anode was abraded.

Anode-Concrete Interfacial Chemistry. The pH of the unaged, uncatalyzed anode-concrete interface was 11.1,Table 5, close to the value of 12 to 13 typical of concrete (Ref 18, 24). The pH of the interface dropped to roughly 6 to 7 with aging, in agreement with changes predicted by anode reactions 1 and 2. The decrease in pH was greatest for the aged, uncatalyzed anode. The decrease represents the loss of hydroxyl ions from the cement paste and the inability of the concrete to buffer these losses at a rate comparable to anode reactions 1 and 2, i.e., the process of acidification. Acidification of the anode-concrete interface for nonconsumeable anodes is well documented (Ref 39 -42) and can result in the deterioration of the cement paste. The efects are strongly dependent upon the anode current density (Ref 39, 40).

Figure 10 shows a BE SEM photomicrograph of a typical aged anode cross section. The titanium anode is the light band at the top of the image. A reaction zone characterized by the loss of cementitious material from the cement paste lies below it. This reaction zone grew in width to 1 to 2 mm as aging progressed. It is a consequence of acidification and results from the dissolution of calcium minerals from the cement paste (Ref 43). Below the reaction zone was a layer of dense concrete where the calcium minerals displaced from the reaction zone are deposited in voids, pores, and cracks. Dense concrete layers surrounding nonconsumable anodes have been reported previously for titanium mesh anodes embedded in concrete (Ref 44).

Figure 11 shows a BE SEM image and element maps for titanium, calcium, and cobalt, obtained by EDS x-ray analyses of the same area for an aged, catalyzed anode. The titanium anode is the bright band across the top of Fig. 11(a) and the corresponding bright band in the titanium element map shown in Fig. 11(b). No migration of titanium into the concrete is evident in Fig. 11(b). Figure 11(c) shows the region identified as the reaction zone. Calcium initially present in the cement paste has been stripped from this zone as a consequence of the anode-concrete interface acidification. The skeletal structure that remains in the reaction zone and supports the aged anode contains insoluble concrete constituents, such as silica and alumina minerals and fine aggregate.

Cracks present in the Ca-deficient, silica-rich reaction zone, Fig. 11(a), extend only the width of the reaction zone and appear to have formed during electrochemical aging. They typically are the site of deepest penetration of the reaction zone into the concrete and probably serve as conduits for moisture and hydrogen ions to the cement paste. Their presence suggests that the silica-rich structure in the reaction zone is brittle and easily damaged. Thus, the low bond strength and increasingly friable nature of the anode with aging is seen to be a consequence of acidification.

NACE Interantional (Ref 45) suggests a maximum anode current density of 108 mA/m^2 (10 mA/ft^2) to prevent significant deterioration of the anode-concrete interface from acidification. This limit may work well for embedded anodes where a 1 to 2 mm thick reaction zone would not affect anode contact with the concrete or structural integrity of the anode installation. However, the volume of cement past relative to anode surface area in a 1 to 2 mm layer surrounding an embedded mesh anode and available to neutralize the products of acidification is 2 to 3 times that for planar thermal sprayed anodes. The impacts of acidification could be mitigated by application of a thin porous mortar overlay on the anode. Presumably this would increase the availability of neutralizing Ca minerals and enhance the appearance of the anode surface without affecting anode operation.

Penetration of the cobalt catalyst into and dispersion throughout the reaction zone is evident in Fig. 11(d). In fact, the highest concentration of cobalt is located primarily at the boundary between the reaction zone and the dense concrete. This suggests that the cobalt catalyst, originally located at the anode-concrete interface, dissolves in the increasingly acid environment of the interface as aging proceeds and disperses into the reaction zone to reprecipitate again as Co_3O_4. It also suggests that the site of anode reactions 1 and 2 becomes more diffuse with dispersion of the catalyst and includes the entire reaction zone. Dispersion of the catalyst away from the anode and into the more basic concrete environment should protect

Table 5 Properties of unaged and aged titanium anodes on concrete

Anode description (a)	Electrochemical age, kC/m^2	Resistivity, $\mu\Omega \cdot cm$	Bond strength, MPa	Interfacial pH
Concrete slabs				
Uncatalyzed, unaged, air	0	2860	1.18	11.1
Catalyzed, unaged, air	0	2570	…	…
Catalyzed, unaged, nitrogen	0	1550	…	…
Uncatalyzed, aged, air	1520	8280	0.01	5.7-5.9
Catalyzed, aged, air	1520	7200	0.26	6.6-6.9
Catalyzed, aged, nitrogen	1520	4310	0.28-0.35	6.2-7.7
Depoe Bay Bridge, zone 14				
Catalyzed, unaged, air	0	3150	…	…
Catalyzed, aged, air	102	3390	…	11.4
Catalyzed, aged, air	215	3650	…	…

(a) substrate, catalysis, aging, and atomizing gas.

the catalyst from the leaching effects of repeated wettings by precipitation, fog, and dew and lead to a longer catalyst life. The stability of the catalyzed anode operating voltage with aging, Fig. 8 and 9, indicates dispersion of the catalyst into the reaction zone and does not adversely affect anode performance.

Figure 12 shows a composition-depth profile for the traverse (arrow) in Fig. 11(a). The region from approximately 0.06 mm (the titanium anode) to 0.65 mm (the reaction front) represents the reaction zone. In this region there is almost no calcium. What remains is a silica-rich zone containing a small amount of alumina. Cobalt is distributed throughout this zone and is present at levels as high as 8 at.%.

Cross sections of the aged, catalyzed anode from the Depoe Bay Bridge were analyzed in the same way as the laboratory anodes. High concentrations of the cobalt catalyst remained at the anode-concrete interface after aging for 146 kC/m^2. Preexisting cracks in the concrete near the anode-concrete interface were filled with precipitates containing cobalt, presumably Co_3O_4.

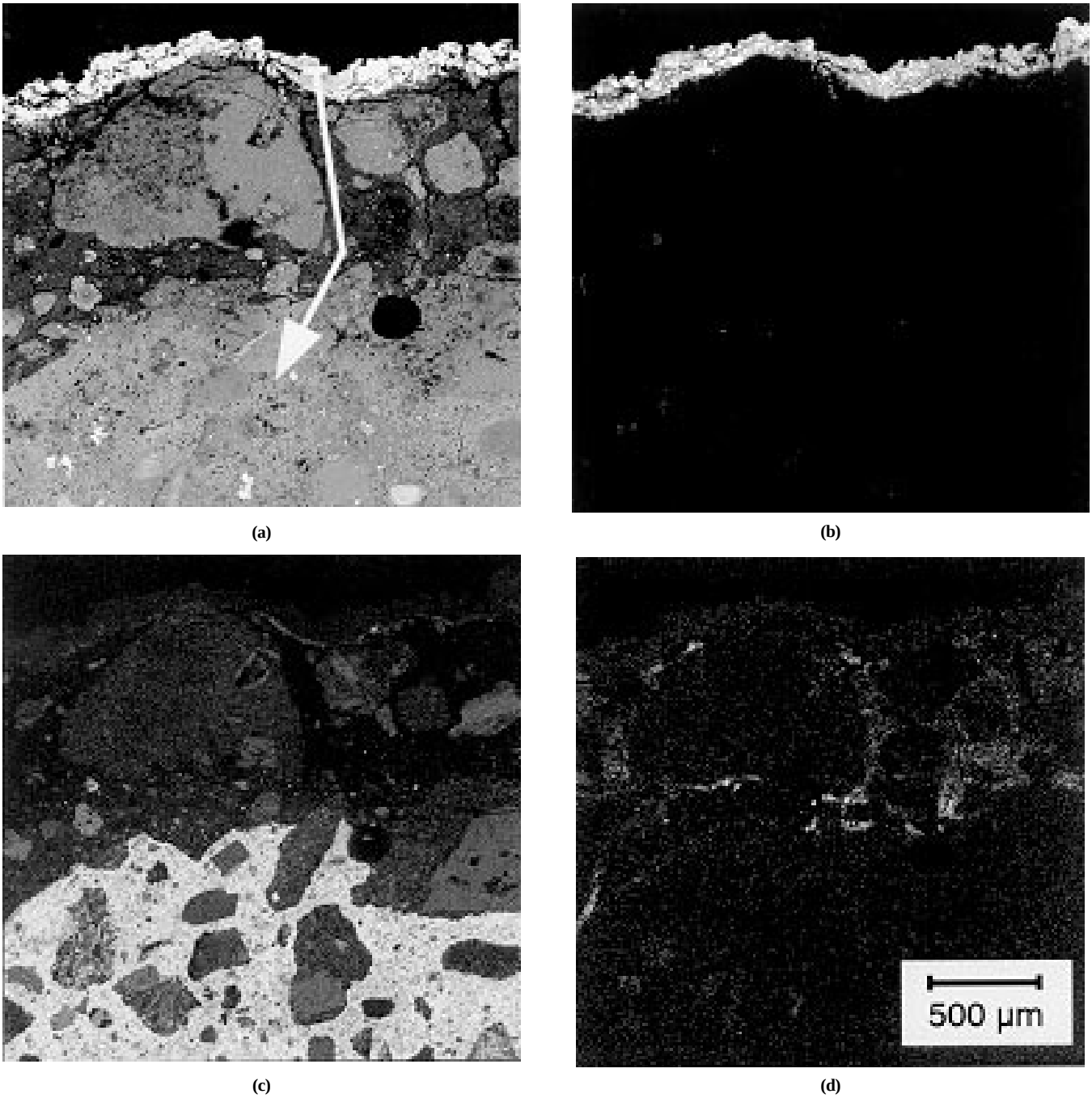

Fig. 11 Cross section of aged, catalyzed anode formed by air atomization. (a) Back-scattered electron scanning electron microscopy image. (b) Ti Kα x-ray map. (c) Ca Kα x-ray map. (d) Co Kα x-ray map. Arrow in Fig. 11(a) is the path of analytical scanning electron microscopy traverse for composition depth profile shown in Fig. 12.

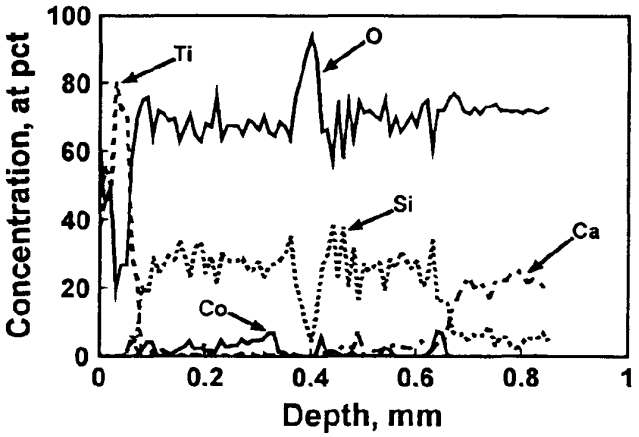

Fig. 12 Composition depth profile for traverse in Fig. 11(a) for aged, catalyzed anode formed by air atomization

Some dispersion of the catalyst into the cement paste occurred during application. There was no evidence beneath the anode of the formation of a reaction zone as seen at the interface of the aged laboratory anodes (Fig. 10 and 11a). However, the measurements in Table 5 show the anode resistivity increased with aging, suggesting that some changes in the bridge anode, analogous to those observed for the laboratory anodes, occurred with aging. The absence of a reaction zone may simply mean more aging must occur for it to be visible by the means used in this study. Another interpretation, of more interest in terms of CP system service life, would suggest that accelerated aging in the laboratory exaggerated the effects of the anode reaction on the anode-concrete interfacial chemistry. In this argument, the low current density used by Oregon DOT for coastal ICCP systems more readily allowed a high pH environment to be maintained at the anode-concrete interface and less structural damage from acidification occurred to the concrete supporting the anode. This would lessen the effects of electrochemical aging on the long term durability of the catalyzed titanium anode and increase the service life of the anode.

4. Conclusions

Thermal sprayed titanium anodes for ICCP of bridges have a porous, heterogeneous structure and heterogeneous composition strongly affected by reactions between the molten titanium spray, atomizing gas, and air. Computed cooling rates for the anode coating were low because titanium has a low thermal conductivity, and concrete is a poor heat sink. These cooling rates ranged from 10 to 150 K/s, well below rates that would lead to rapid solidification.

Reactions with the atomizing gas and atmosphere produce coatings consisting of α-titanium containing high levels of interstitial oxygen and nitrogen, and a fcc phase thought to be Ti(O,N) with nonmetallic lattice sites occupied by oxygen and nitrogen. Composition gradients within individual splats resulted in α-titanium-rich and Ti(O,N)-rich regions with microstructures produced by equilibrium processes at the solidification front and strongly dependent upon composition. The α-titanium-rich and Ti(O,N)-rich regions typically appeared as a layered structure in the completed anode, with the Ti(O,N)-rich regions typically representing the splat skin at the time of impact. Cracks originated in the Ti(O,N)-rich regions, paralleling the layer interface, with secondary cracks across α-titanium-rich regions, connecting other primary cracks. Anode resistivity was governed by the heterogeneous splat composition and structure. Anodes produced by N_2 atomization had more uniform composition, less cracking, and lower resistivity than those produced by air atomization.

Electrochemical aging of catalyzed anodes substantially lowered the pH of the anode-concrete interface due to acidification resulting from the anode reactions. This led to etching of concrete at the anode-concrete interface and loss of calcium from the associated cement paste, producing an ever-widening Ca deficient, silica-rich reaction zone at the interface. The silica-rich structure that remained was brittle, readily cracked, and was damaged by abrasion. Anode bond strength and durability was reduced over time with the formation of this reaction zone. However, anode losses from the concrete did not occur except when the anode was abraded. Aged anodes produced using N_2 atomization exhibited lower resistivity and marginally higher bond strengths than anodes produced using air atomization. Aged, uncatalyzed anodes had substantially lower bond strengths and higher anode resistivities than aged, catalyzed anodes.

Cobalt catalyst, applied to the anode as an aqueous cobalt nitrate-amine complex, penetrated the anode and accumulated at the anode-concrete interface and in cracks within the concrete adjacent to the interface. Anodic polarization during and after application converted the cobalt to the active catalyst, Co_3O_4. With aging, cobalt catalyst dissolved in the increasingly acid environment of the interface and dispersed into the Ca-deficient, silica-rich reaction zone to reprecipitate and form a more diffuse site for the anode reactions. Catalyzed titanium anodes performed well over a wide range of humidity (30 to 100% RH) with little change in operating voltage at a constant current density. Stable operation of catalyzed anodes was maintained for a period equivalent to 23 years service (1520 kC/m^2) at Oregon DOT bridge ICCP conditions with no evidence that operation would degrade with further aging. Early results from the field experiment at the Depoe Bay Bridge suggest anodes may age more slowly at low current densities with lesser impact from acidification.

References

1. O. Kubaschewski and B.E. Hopkins, *Oxidation of Metals and Alloys*, Butterworths, 1962, p 5-14, 24
2. M.L. Allan, Probability of Corrosion Induced Cracking in Reinforced Concrete, *Cem. Concr. Res.*, Vol 25 (No. 6), 1995, p 1179-1190
3. C.J. Mudd, G.L. Mussinelli, M. Tettamanti, and P. Pediferri, Cathodic Protection of Steel in Concrete, *Mater. Perform.*, Vol 27 (No. 9), 1988, p 18-24
4. R.A. Carello, D.M. Parks and J.A. Apostolos, *Development, Testing and Field Application of Metallized Cathodic Protection Coatings on Reinforced Concrete Substructures*, California Department of Transportation, FHWA/CA/TL-89/04, May 1989, 100 p
5. B.S. Covino, Jr., S. Bullard, G.R. Holcomb, S.D. Cramer, G.E. McGill, and C.B. Cryer, Bond Strength of Electrochemically-Aged Arc-Sprayed Zinc Coatings on Concrete, Paper 96308, *Corrosion '96*, NACE International, Houston, 1996, 17 p

6. B.S. Covino, Jr., S.J. Bullard, G.R. Holcomb, S.D. Cramer, G.E. McGill, and C.B. Cryer, Factors Affecting the Bonding of Arc-Sprayed Zinc to Concrete, *Balancing Economics and Compliance for Maintaining Protective Coatings*, SSPC 95-09, Steel Structures Painting Council, 1995, p 115-128
7. B.S. Covino, Jr., S.J. Bullard, G.R. Holcomb, S.D. Cramer, G.E. McGill, and C.B. Cryer, Bond Strength of Electrochemically-Aged Arc-Sprayed Coatings on Concrete, *Corrosion*, Vol 53 (No. 5), 1997, p 399-411
8. B.S. Covino, Jr., S.D. Cramer, S.J. Bullard, G.R. Holcomb, G.E. McGill, and C.B. Cryer, Factors Affecting Thermal-Sprayed Zinc Anodes on Concrete, Paper 173, *Proc. 13th Intern. Corrosion Congress*, Australasian Corr. Assoc., 1996, 7 p
9. G.R. Holcomb, S.J. Bullard, B.S. Covino, Jr., S.D. Cramer, C.B. Cryer, and G.E. McGill, Electrochemical Aging of Thermal-Sprayed Zinc Anodes on Concrete, *Proc. 9th National Thermal Spray Conference*, ASM International, 1996, p 185-192
10. B.S. Covino, Jr., S.D. Cramer, S.J. Bullard, G.R. Holcomb, W.K. Collins, and G.E. McGill, Consumable and Non-Consumable Thermal Spray Anodes for Impressed Current Cathodic Protection of Reinforced Concrete Structures, Paper 98658, *Corrosion '98*, NACE International, Houston, 1998, 17 p
11. S.J. Bullard, B.S. Covino, Jr., G.R. Holcomb, S.D. Cramer and G.E. McGill, Bond Strength of Thermal-Sprayed Zinc on Concrete during Early Electrochemical Aging, Paper 97232, *Corrosion '97*, NACE International, Houston, 1997, 17 p
12. J.E. Bennett, T.J. Schue, and G. McGill, Protecting Reinforced Concrete using Thermal-Sprayed Titanium Anodes, *Mater. Perform.*, Vol 34 (No. 11), 1995, p 23-27
13. R. Brousseau, B. Arsenault, S. Dallaire, D. Rogers, T. Mumby, and D. Dong, Sprayed Titanium Coatings for the Cathodic Protection of Reinforced Concrete, *J. Therm. Spray Technol.*, Vol 7 (No. 2), 1998, p 193-196
14. G.E. McGill, S.D. Cramer, B.S. Covino, Jr., G.R. Holcomb, S.J. Bullard, W.K. Collins, R.D. Govier, and R.D. Wilson, "Field Application of a Thermal -Sprayed Titanium Anode for Cathodic Protection of Reinforcing Steel in Concrete—Final Report, "FHWA-OR-RD-99-13, Federal Highway Administration, U.S. Department of Transportation, Washington D.C., Jan 1999, 123 p
15. G.R. Holcomb, S.D. Cramer, S.J. Bullard, B.S. Covino, Jr., W.K. Collins, R.D. Govier, and G.E. McGill, Characterization of Thermal-Sprayed Titanium Anodes for Cathodic Protection, *Thermal Spray: A United Forum for Scientific and Technological Advances*, ASM International, 1997, p 141-150
16. B.S. Covino, Jr., S.D. Cramer, G.R. Holcomb, S.J. Bullard, W.K. Collins, and G.E. McGill, Characterization of Electrochemically-Aged Thermal-Spray Titanium Anodes on Concrete, *Thermal Spray: A United Forum for Scientific and Technological Advances*, ASM International, 1997, p 151-160
17. R.P. Krepski, *Thermal Spray Coating Applications in the Chemical Process Industries*, Materials Technology Institute, Pub. 42, NACE International, Houston, 1993, p 16
18. B.S. Covino, Jr., S.J. Bullard, S.D. Cramer, G.R. Holcomb, G.E. McGill, C.B. Cryer, A. Stoneman, and R.R. Carter, Interfacial Chemistry of Zinc Anodes for Reinforced Concrete Structures, Paper 97233, *Corrosion '97*, NACE International, Houston, 1997, 20 p
19. Oxygen-Titanium Alloy Phase Diagram, *Alloy Phase Diagrams*, Vol 3, *ASM Handbook*, ASM International, 1992, p 2-324
20. Nitrogen-Titanium Alloy Phase Diagram, *Alloy Phase Diagrams*, Vol 3, *ASM Handbook*, ASM International, 1992, p 2-299
21. F.A. Cotton and G. Wilkinson, *Advanced Inorganic Chemistry*, Interscience, New York, 1966, p 51
22. A.F. Wells, *Structural Inorganic Chemistry*, Oxford University Press, 1962, p 166
23. A.A. Balandin, A. Bielanski, G.K. Boreskov, et al., *Catalysis and Chemical Kinetics*, Academic Press, 1964, p 60-73
24. S.J. Bullard, S.D. Cramer, B.S. Covino, Jr., G.R. Holcomb, G.E. McGill, and R. Reis, Thermal-Sprayed Zinc Anodes—Laboratory and Field Studies, *Expanding Coatings Knowledge Worldwide*, SSPC 97-09, Steel Structures Paint Council, 1997, p 309-319
25. E.O. McLean, Soil pH and Lime Requirement, *Methods of Soil Analysis, Part 2—Chemical and Microbiological Properties*, A.L. Page, Ed., American Society of Agronomy, Madison, WI, 1982, p 206-209
26. J.P. Bars, D. David, E. Etchessahar, and J. Debuigne, Titanium-α Nitrogen Solid Solution Formed by High Temperature Nitriding: Diffusion of Nitrogen, Hardness, and Crystallographic Parameters, *Metall. Trans. A*, Vol 14, Aug 1983, p 1537-1543
27. E. Etchessahar, J. P. Bars, and J. Debuigne, The Ti-N System: Equilibrium between the δ, ε, and α Phases and the Conditions of Formation of the Lobier and Marcon Metastable Phase, *J. Less-Common Metals*, Vol 134, 1987, p 123-139
28. E.S. Bumps, H.D. Kessler, and M. Hansen, The Titanium-Oxygen System, *Trans. ASM*, Vol 45, 1953, p 1008-1028
29. Crystal Ionic Radii of the Elements, *Handbook of Chemistry and Physics*, 60th ed., R.C. Weast, Ed., 1979-1980, p F-214
30. J. Chastain, Ed., *Handbook of X-Ray Photoelectron Spectroscopy*, Perkin-Elmer, 1992, 261 p
31. N. F. Mott and H. Jones, *The Theory and the Properties of Metals and Alloys*, Dover, New York, 1958, p 245-249
32. C. A. Wert and R. M. Thomson, *Physics of Solids*, McGraw-Hill, 1970, p 222-250
33. S.A. David and J.M. Vitek, Correlation between Solidification Parameters and Weld Microstructure, *Int. Mater. Rev.*, Vol 34 (No. 5), 1989, p 213-245
34. C.M. Adams, Jr. and C.E. Jackson, Heat Flow in Welding, *Welding Handbook*, Vol 1, 7th ed., American Welding Society, 1976, p 84
35. L.E. Collins, Overview of Rapid Solidification Technology, *Can. Metall. Q.*, Vol 25 (No. 1), 1986, p 59-72
36. K. Hauffe, *Oxidation of Metals*, Plenum Press, 1965, p 209-228
37. O. Kubaschewski and B.E. Hopkins, *Oxidation of Metals and Alloys*, Butterworths, 1962, p 213-217
38. G. Gusmano, A. Bianco, G. Montesperelli, and E. Traversa, *Electrochim. Acta*, Vol 41 (No. 7/8), 1996, p 1359-1368
39. P. Pedeferri and M. Tettamanti, Long Term Tests on Cathodic Protection of Steel in Concrete with Mixed Metal Oxides Activated Titanium Anode Net, *Proc. Fifth Middle East Corrosion Confererence*, 28-30 Oct 1991, (Manama, Bahrain), The Bahrain Society of Engineers, 1991, p 272-282
40. P. Pedeferri, G.L. Mussinelli, M. Tettamanti, and C.J. Mudd, Cathodic Protection of Steel in Concrete with Expanded Titanium Anode Net System, *U. K. Corrosion 89*, 8-10 Nov, 1989 (Blackpool, United Kingdom) The Institution of Corrosion Science and Technology/Corrosion Engineering Association, Vol 3, 1989, p 3-181 to 3-198
41. P.C.S. Hayfield and M.A. Warne, Titanium Based Mesh Anode in the Cathodic Protection of Reinforcing Bars in Concrete, *Constr. and Build. Mater.*, Vol 3 (No 3), Sept 1989, p 152-158
42. K. Nielsen-Dharmaratne and F.O. Gronvold, Internal Anodes in Concrete Structures, Mater. Perform., Vol 31 (No 6), June 1992, p 29-32
43. M. Pourbaix, *Atlas of Electrochemical Equilibria*, NACE International, Houston, 1974, p 147-150
44. C.J. Weale, "Cathodic Protection of Reinforced Concrete: Anodic Processes in Cements and Related Electrolytes," Thesis No. DX185652, The British Library, 1992, 415 p
45. "Cathodic Protection of Reinforcing Steel in Atmospherically Exposed Concrete Structures," NACE Standard RP0290-90, NACE International, Houston , 1990